In situ realization of particlelike scattering states in a microwave cavity

Julian Böhm,[1] Andre Brandstötter,[2] Philipp Ambichl,[2] Stefan Rotter,[2] and Ulrich Kuhl[1]

[1]*Université Côte d'Azur, CNRS, Institut de Physique de Nice (InPhyNi), F-06108 Nice, France, EU*
[2]*Institute for Theoretical Physics, Vienna University of Technology (TU Wien), A-1040 Vienna, Austria, EU*

We realize scattering states in a lossy and chaotic two-dimensional microwave cavity which follow bundles of classical particle trajectories. To generate such particlelike scattering states, we measure the system's complex transmission matrix and apply an adapted Wigner-Smith time-delay formalism to it. The necessary shaping of the incident wave is achieved *in situ* using phase- and amplitude-regulated microwave antennas. Our experimental findings pave the way for establishing spatially confined communication channels that avoid possible intruders or obstacles in wave-based communication systems.

Introduction. The propagation of waves in complex media is widely studied in physics [1]. To probe the scattering properties of a medium, one typically uses well-defined incident waves and measures their spatial profile at the output. However complex the scattering process may be, the output stays deterministically related to the input such that any change in the input parameters can be directly related to changes in the output pattern. This deterministic relation is encapsulated in a system's scattering matrix [2] whose massive information content is exploited through wavefront shaping [3–5]. The basic idea in this emerging field is to manipulate the incident waves in such a way that a certain output is achieved. This concept was pushed forward due to the possibility of sufficient input control. Spatial light modulators in optics [6–9], IQ modulators or spatial microwave modulators in the microwave field [10–12], and transducers in acoustics [13] offer the possibility to use this concept in a large variety of physical disciplines.

Early goals were the development of new schemes for the focusing or defocusing of waves and the compression of pulses [3,14–17] *behind* a disordered slab. Special wave patterns can also be achieved *within* such a medium like for states that are spatially focused on an embedded target [18–20]. In multimode fibers also so-called principal modes were recently generated that are focused in time both at the input and the output facet of the fiber [21–23]. States with the unique feature of remaining focused both in space and time during the entire propagation through a complex medium are the so-called particlelike scattering states (PSSs) [24]. Their spatial collimation makes sure that they are both very robust and tap-proof against perturbations or eavesdropping in those regions that they do not explore. Additionally, the facts that PSSs are fully transmitted even across complex scattering structures and that they remain focused when reaching a desired receiver guarantee that all the information they carry ends up securely where it should. Finally, the association of PSSs with the smallest possible time delays assures that the information transfer is as fast as possible and unwanted dissipation to the environment is minimal.

A first experimental realization using elastic waves in a cavity and a disordered waveguide have been presented in

Ref. [25], where the states were obtained by a numerical synthesis of experimentally measured system excitations. Here we present an *in situ* microwave realization (see Fig. 1) of such PSSs by means of an active input shaping, thus generating and detecting the PSSs directly. As microwaves are being widely used for information transfer, we anticipate that our proof-of-principle demonstration also has technological relevance. Additionally, the realization scheme presented here is solely based on the system's complex transmission matrix T rather than on the whole scattering matrix S as originally proposed in Ref. [24] and used in Ref. [25]. Moreover, our experiment shows that the intrinsic losses as well as the experimental noise still allow us to generate PSSs.
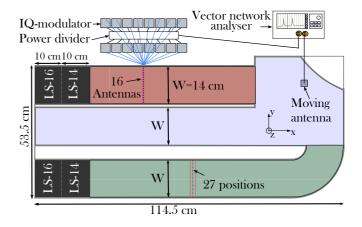

FIG. 1. Sketch of the experimental setup. A two-dimensional microwave cavity is excited by 16 monopole antennas (left upper corner) placed in the incoming lead (red-colored area). The antennas are connected to IQ modulators controlling amplitude and phase of the microwave signal, whereas the IQ modulators themselves are fed by a vector network analyzer. The chaotic scattering region (light blue area) is connected to the incoming lead and an outgoing one (green area). Both leads are closed by absorbing foam material (LS-14, LS-16). The dotted line in the exit lead indicates the 27 positions where the movable monopole antenna is placed for the measurement of the complex transmission matrix T. The red square in the exit lead marks the area for the computation of I_{ob} and I_{em} (see text).

Theory. We start by introducing the Wigner-Smith time-delay matrix (WSTDM) $Q = -i S^{-1} dS/d\omega$ (involving a frequency derivative), which is an established tool for measuring the time delay associated with the scattering of a wave packet in a system [26–28] featuring also interesting connections to the system's density of states [29–32]. The WSTDM is Hermitian for unitary scattering systems (for which $S^{\dagger} S = \mathbb{1}$), thus resulting in real eigenvalues τ_n (n represents the nth eigenvalue), also called proper delay times. The corresponding eigenvectors $\vec{u}_n$ (given as a coefficient vector in a certain basis) are known as principal modes [33] and have the remarkable feature of being insensitive (to first order) to small changes of their input frequency—in the sense that the spatial output profile $\vec{v}_n = S\vec{u}_n$ does not change (up to a global factor). This property is especially useful for dispersion-free propagation through multimode fibers [21,22,34,35] and is mathematically expressed as

$$\vec{v}_n(\omega_0 + \Delta\omega) \approx \exp(i\tau_n\Delta\omega)\vec{v}_n(\omega_0), \quad (1)$$

where $\Delta\omega$ is the change in frequency and ω_0 is the frequency at which $\vec{u}_n$ is evaluated. The global phase factor $\exp(i\tau_n\Delta\omega)$ is determined by the corresponding eigenvalue τ_n. In Ref. [24], it was demonstrated that a certain subclass of principal modes have a particlelike wave function resembling a focused beam. These PSSs live in the subspace of fully transmitted or fully reflected states, just like a particle that can either traverse the scattering region or be reflected back at some boundary or obstacle. In this work, we investigate PSSs that get fully transmitted through a microwave cavity as shown in Fig. 1.

As in most experiments, we also do not have access to the full scattering matrix S. We thus use a modified WSTDM where we replace the scattering matrix S by the complex transmission matrix T, which is accessible in our experimental setup. In the following, we show that only the knowledge of T is sufficient to find PSSs connecting the input to the output. The eigenvalue equation for the nth eigenvector $\vec{q}_n$ of this new operator q reads as follows:

$$q_n = -i\, T^{-1}(\omega)\frac{dT(\omega)}{d\omega}\vec{q}_n = \lambda_n\vec{q}_n, \quad (2)$$

where λ_n is the eigenvalue. An ordinary inverse of T appearing in Eq. (2) does not exist if T is nonquadratic or singular. In the Supplemental Material [36], we introduce an effective inverse that still allows for the calculation of q. Contrary to eigenstates of the Hermitian operator Q, here only the transmitted output profile $\vec{o}_n = T\vec{q}_n$ is insensitive (up to a global factor) with respect to a change of the input frequency ω, since the operator q involves only T. This translates into

$$\vec{o}_n(\omega_0 + \Delta\omega) \approx \exp(i\lambda_n\Delta\omega)\,\vec{o}_n(\omega_0). \quad (3)$$

One can analytically derive (see Ref. [33]) an expression for the complex eigenvalues

$$\lambda_n = \frac{d\phi_n}{d\omega} - i\frac{d\ln(|co_n|)}{d\omega}, \quad (4)$$

where ϕ_n is the transmitted global phase, i.e., $\vec{o}_n = |\vec{o}_n|e^{i\phi_n}\hat{o}_n$ ($\hat{o}_n$ is the unit vector of $\vec{o}_n$). The real part $\mathrm{Re}(\lambda_n)$ reflects the frequency derivative of the scattering phase and is therefore proportional to the time delay [26] of the eigenstate $\vec{q}_n$. The imaginary part $\mathrm{Im}(\lambda_n)$ describes how the transmitted intensity $|\vec{o}_n|^2$ changes with respect to a change of the

frequency ω as can be seen from Eq. (3), $|\vec{o}_n(\omega_0 + \Delta\omega)|^2 \approx \exp[-2\mathrm{Im}(\lambda_n)\Delta\omega]\,|\vec{o}_n(\omega_0)|^2$. In order to identify PSSs among all the other eigenstates $\vec{o}_n$, we make use of the corresponding eigenvalues λ_n. Since PSSs are highly collimated and are not distributed all over the scattering region, the time it takes a PSS to traverse the scattering region is typically much smaller than for other scattering states that get scattered multiple times inside the scattering region. Because $\mathrm{Re}(\lambda_n)$ measures this scattering time, i.e., the time delay, PSSs can be identified by a small value of $\mathrm{Re}(\lambda_n)$. Furthermore, PSSs feature a small $\mathrm{Im}(\lambda_n)$, since for fully transmitting and spatially confined scattering states the transmitted intensity barely changes with input frequency ω as compared to states that get scattered multiple times.

Setup. The scattering setup with which we investigate the appearance of PSSs is shown in Fig. 1. A chaotic scattering region is attached to an incoming lead and an outgoing lead (see red, light blue, and green areas in Fig. 1, respectively). The width of the lead W of 14 cm allows the propagation of 16 transverse-electrical modes (TE modes) in the entrance and the exit lead at the working frequency of $\nu_0 = \omega_0/2\pi = 17.5$ GHz which corresponds to a wavelength in air of 1.71 cm. These 16 modes are excitable via 16 antennas. Each antenna is connected to one IQ modulator, which controls amplitude and phase of the microwave signal passing through. The IQ modulators themselves are fed by a vector network analyzer (VNA, Agilent E5071C) connected to a power splitter (Microot MPD16-060180). The used connecting cables, connectors, and antennas are all identical to avoid different propagation phases. The ends of the waveguide are filled with absorbing foam material (types: LS-14 and LS-16 from Emerson & Cuming) to reduce reflections.

The cavity is placed under a metallic plate featuring a 5×5 mm^2 grid of holes (hole radius of 2 mm). Working below the cutoff frequency of 18.75 GHz guarantees to excite only the fundamental TE mode, i.e., TE$_0$, where the z component of the electric field E_z is constant with respect to z and the x,y components $E_{x,y}$ are zero. The grid of holes in the top plate closing the cavity enables us to introduce a movable monopole antenna which measures E_z at any given hole position in the cavity as in previous experiments [37,38]. The holes can also be used to insert cylindrical obstacles (aluminum, radius: 2 mm) leading to additional scattering within the cavity (see also Refs. [12,20]). The scattering setup was chosen such that the incoming and outgoing leads support a sufficient number of modes. The long middle part (located between incoming and outgoing leads) serves as verification that PSSs avoid this region whereas arbitrary scattering states typically enter this part.

Experimental results. To obtain the q operator experimentally, we measure $T(\omega)$ within a frequency window around the working frequency. To reduce noise effects, we perform a Fourier filtering (see Supplemental Material [36]) before extracting the Wigner-Smith time-delay operator. This is particularly helpful to stabilize the derivative of the measured complex T matrix. The positions where the microwave signal (16 antennas connected to the IQ modulators) is injected and transmission is measured with the moving antenna (27 positions) are marked in Fig. 1. (Taking into account 27 instead of 16 points allows us to stabilize the experimentally obtained

eigenvalues against noise and experimental imperfections.) Since T is thus a rectangular matrix of size 27×16, we cannot calculate its ordinary inverse to construct the q-operator. Using the technique described in the Supplemental Material [36], we work with the operator $\tilde{q}$ which only includes a subpart of T associated to a certain number η of highly transmitting channels. We tested empirically that the best results for PSSs, i.e., small $\text{Im}(\lambda_n)$, are obtained for the highest $\eta = 7$ transmitting channels for the calculation of $\tilde{q}$. Once these eigenstates of $\tilde{q}$ are evaluated, we inject them and verify their particlelike shape using the movable antenna that enters the cavity through the holes in the top plate. At first we investigate the eigenstate featuring the smallest value of $\text{Re}(\lambda_n)$, i.e., the shortest time delay. The result of this measurement is shown as particlelike scattering state 1 (PSS 1) in Fig. 2(a). The wave function shows the predicted behavior of following the shortest trajectory bundle connecting the incoming with the outgoing lead [see red bundle in Fig. 2(b), left].

Next, we investigate PSSs with larger time delays, which correspond to the green and the blue classical trajectory bundles shown in Fig. 2(b). It turns out that the center trajectories of these two bundles have almost the same length ($L_2 = 50.0$ cm and $L_3 = 49.1$ cm). Since similar path lengths lead to similar time delays, the operator q cannot fully discriminate between these two scattering states. While PSS 2 corresponds quite well to the green classical bundle, PSS 3 mixes both bundles, green and blue. In other words, the measured q eigenstates corresponding to these bundles are in a near-degenerate superposition with path contributions of both lengths (L_2 and L_3) showing up in their wave functions. Demixing degenerate PSSs can be achieved by analyzing a state's contributions in the angular mode basis, as numerically shown in the Supplemental Material [36].

As comparison, we show in Fig. 2(c) the intensity distribution of a state governed by exciting only a single randomly chosen antenna [further referred as RSS]. We see that also the RSS shows some intensity maxima within the cavity; however, these maxima do not follow classical trajectory bundles between incoming and outgoing leads. Moreover, the RSS extends into the middle part of the scattering region, which is avoided by all PSSs.

The RSS also shows a significantly lower spectral robustness of its transverse output profile which we define as

$$\text{Corr}(\nu) = \frac{|\vec{o}^\dagger(\nu) \cdot \vec{o}(\nu_0)|}{|\vec{o}(\nu)||\vec{o}(\nu_0)|} \quad \text{with} \quad \vec{o}(\nu) = T(\nu)\vec{i}, \quad (5)$$

where $\vec{i}$ is the random input state. Equation (5) is the normalized correlation between the output vector $\vec{o}$ at frequency ν compared to its output at ν_0 (the frequency at which the states are evaluated). PSS 1 is the state showing the highest output robustness when compared to the other PSSs (see Fig. 3). Since PSS 2 and PSS 3 perform a reflection at the convex cavity boundary, they are considerably more sensitive with respect to small changes in the frequency in terms of the output robustness when compared to PSS 1, which is transmitted entirely without any boundary reflections. This explains why the correlation curve in Fig. 3 of PSS 1 is flatter than the one of PSS 2 and 3. The correlation of the random state RSS is, as expected, the lowest.

(a) Particlelike state 1 (PSS 1)

Particlelike state 2 (PSS 2)

Particlelike state 3 (PSS 3)

(b) Trajectory bundles
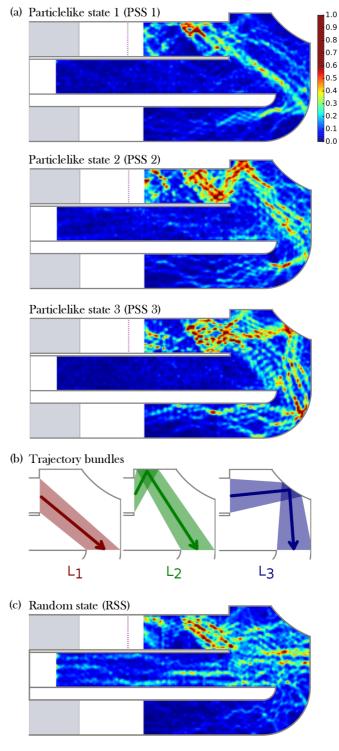
L_1 L_2 L_3

(c) Random state (RSS)

FIG. 2. (a) Intensity of the particlelike scattering states which are experimentally created by wave-front shaping of the incident wave in the left upper lead. (b) Central path length of the corresponding classical trajectory bundles of the particlelike scattering states ($L_1 = 33.3$ cm, $L_2 = 50.0$ cm, $L_3 = 49.1$ cm). (c) Typical intensity distribution when only one single antenna is excited (here: second antenna from top). Note that the intensities in panels (a) and (c) are normalized each to a maximum (minimum) value of 1 (0).

As PSSs wave functions are highly collimated on bundles of classical particle trajectories of similar length, putting
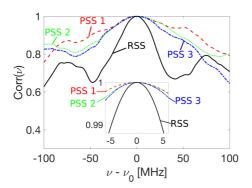
FIG. 3. Autocorrelation function of the output profile of the three particlelike scattering states (PSS) and the random scattering state (RSS) according to Eq. (5). All three PSSs are more stable with respect to a change of the incident frequency ν as compared to the RSS.

FIG. 4. (a) Change of the transmitted intensity ΔI_{rel} of the particlelike scattering states (PSS) and the random state while moving the rhombic obstacle between position 1 (Pos 1) to position 5 (Pos 5) [see panel (b)] operating at the center frequency $\nu_0 = 17.5$ GHz. PSS 1 and PSS 2 show a significant drop at only one position where the obstacle crosses the classical trajectory bundle. As expected, PSS 3, which is a superposition of two classical bundles, is affected by all obstacle positions. The RSS shows no indication of a particlelike pattern.

an obstacle in the way of such a trajectory, the observed transmission for a corresponding PSS drops down, whereas putting an obstacle outside of the occupied region of the PSS affects the wave function only slightly. To test this idea explicitly experimentally, we place altogether 13 cylindrical obstacles forming a rhombic shape into the scattering region of the cavity [see Fig. 4(b)]. The obstacles have an equidistant spacing of about 3.3 wavelengths to make sure that their perturbations are uncorrelated. The relative change they induce in the transmitted intensity is evaluated as

$$\Delta I_{rel} = \frac{(I_{ob} - I_{em})}{I_{em}}, \qquad (6)$$

where I_{ob} is the transmitted intensity when the obstacle is placed inside the system and I_{em} is the transmitted intensity for the empty cavity with no obstacle present. The intensities I_{ob} and I_{em} are obtained by computing the sum of the measured transmitted intensities at 135 positions covering the whole width of the outgoing lead indicated by a red square in Fig. 1. As expected, we observe that the PSSs are affected by a strong drop of 30% or more of the transmitted intensity when the scatterer is placed within the bundle supporting the PSS [see Fig. 4(a)]. This observation is interesting from a practical point of view if one aims to transmit intensity from input to output lead in the presence of obstacles. Once a specific PSS is blocked, one can maintain efficient transmission by switching to another PSS (e.g., from PSS 1 to PSS 2), an option that will not work when operating with random scattering states. PSSs will thus be affected only by those local perturbation that fall within the small volume they occupy, which is strongly reduced as
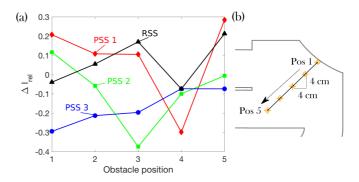
compared to the total cavity volume. Also global perturbations (like uniform cavity absorption) will affect these states much less due to their short delay times.

Conclusions. We perform an *in situ* realization of particlelike scattering states by means of incident wave-front shaping. Particlelike scattering states follow bundles of classical trajectories of similar length and can be identified with the help of the Wigner-Smith time-delay formalism based on a prior measurement of the frequency-dependent transmission matrix $T(\nu)$. We extract three different particlelike scattering states corresponding to three different classical trajectory bundles connecting the input with the output lead attached to a chaotic microwave cavity. Switching between these path bundles can augment the transmission in case one of them is blocked by an obstacle. Our results can also be mapped onto other wave-based systems (acoustic, electromagnetic, quantum, etc.) leading to many possible applications related to efficient, robust, and focused transmission through complex environments [39,40]. We expect that our protocol unfolds its full potential in those domains where many modes can be controlled (as, e.g., in optics).

[1] E. Akkermans and G. Montambaux, *Mesoscopic Physics of Electrons and Photons* (Cambridge University Press, Cambridge, UK, 2007).

[2] S. M. Popoff, G. Lerosey, R. Carminati, M. Fink, A. C. Boccara, and S. Gigan, Measuring the Transmission Matrix in Optics: An Approach to the Study and Control of Light Propagation in Disordered Media, Phys. Rev. Lett. **104**, 100601 (2010).

[3] I. M. Vellekoop and A. P. Mosk, Focusing coherent light through opaque strongly scattering media, Opt. Lett. **32**, 2309 (2007).

[4] A. P. Mosk, A. Lagendijk, G. Lerosey, and M. Fink, Controlling waves in space and time for imaging and focusing in complex media, Nat. Photon. **6**, 283 (2012).

[5] S. Rotter and S. Gigan, Light fields in complex media: Mesoscopic scattering meets wave control, Rev. Mod. Phys. **89**, 015005 (2017).

[6] A. Gehner, M. Wildenhain, H. Neumann, J. Knobbe, and O. Komenda, MEMS analog light processing: An enabling technology for adaptive optical phase control, Proc. SPIE **6113**, 61130K (2006).

[7] E. G. van Putten, I. M. Vellekoop, and A. P. Mosk, Spatial amplitude and phase modulation using commercial twisted nematic lcds, Appl. Opt. **47**, 2076 (2008).

[8] Ernst Lueder, *Liquid Crystal Displays: Addressing Schemes and Electro-optical Effects* (John Wiley and Sons, New York, 2010).

[9] C. Maurer, A. Jesacher, S. Bernet, and M. Ritsch-Marte, What spatial light modulators can do for optical microscopy, Laser Photon. Rev. **5**, 81 (2011).

[10] B. E. Henty and D. D. Stancil, Multipath-Enabled Super-Resolution for rf and Microwave Communication using Phase-Conjugate Arrays, Phys. Rev. Lett. **93**, 243904 (2004).

[11] N. Kaina, M. Dupré, M. Fink, and G. Lerosey, Hybridized resonances to design tunable binary phase metasurface unit cells, Opt. Exp. **22**, 18881 (2014).

[12] J. Böhm and U. Kuhl, Wave front shaping in quasi-one-dimensional waveguides, in *Proceedings of the 2016 IEEE Metrology for Aerospace (MetroAeroSpace)* (IEEE, Piscataway, NJ, 2016), pp. 182–186.

[13] M. Fink, Time reversed acoustics, Phys. Today **50**(3), 34 (1997).

[14] G. Lerosey, J. de Rosny, A. Tourin, and M. Fink, Focusing beyond the diffraction limit with far-field time reversal, Science **315**, 1120 (2007).

[15] O. Katz, E. Small, Y. Bromberg, and Y. Silberberg, Focusing and compression of ultrashort pulses through scattering media, Nat. Photon. **5**, 372 (2011).

[16] D. J. McCabe, A. Tajalli, D. R. Austin, P. Bondareff, I. A. Walmsley, S. Gigan, and B. Chatel, Spatio-temporal focusing of an ultrafast pulse through a multiply scattering medium, Nat. Commun. **2**, 447 (2011).

[17] A. M. Weiner, Ultrafast optics: Focusing through scattering media, Nat. Photon. **5**, 332 (2011).

[18] B. Judkewitz, Y. M. Wang, R. Horstmeyer, A. Mathy, and C. Yang, Speckle-scale focusing in the diffusive regime with time reversal of variance-encoded light (TROVE), Nat. Photon. **7**, 300 (2013).

[19] I. M. Vellekoop, E. G. van Putten, A. Lagendijk, and A. P. Mosk, Demixing light paths inside disordered metamaterials, Opt. Express **16**, 67 (2008).

[20] P. Ambichl, A. Brandstötter, J. Böhm, M. Kühmayer, U. Kuhl, and S. Rotter, Focusing Inside Disordered Media with the Generalized Wigner-Smith Operator, Phys. Rev. Lett. **119**, 033903 (2017).

[21] J. Carpenter, B. Eggleton, and J. Schröder, Observation of Eisenbud-Wigner-Smith states as principal modes in multimode fibre, Nat. Photon. **9**, 751 (2015).

[22] W. Xiong, P. Ambichl, Y. Bromberg, B. Redding, S. Rotter, and H. Cao, Spatiotemporal Control of Light Transmission Through a Multimode Fiber with Strong Mode Coupling, Phys. Rev. Lett. **117**, 053901 (2016).

[23] P. Ambichl, W. Xiong, Y. Bromberg, B. Redding, H. Cao, and S. Rotter, Super- and Anti-Principal Modes in Multi-Mode Waveguides, Phys. Rev. X **7**, 041053 (2017).

[24] S. Rotter, P. Ambichl, and F. Libisch, Generating Particlelike Scattering States in Wave Transport, Phys. Rev. Lett. **106**, 120602 (2011).

[25] B. Gérardin, J. Laurent, P. Ambichl, C. Prada, S. Rotter, and A. Aubry, Particlelike wave packets in complex scattering systems, Phys. Rev. B **94**, 014209 (2016).

[26] L. Eisenbud, The formal properties of nuclear collisions, Ph.D. thesis, Princeton University, Princeton, NJ, 1948.

[27] E. Wigner, Lower limit for the energy derivative of the scattering phase shift, Phys. Rev. **98**, 145 (1955).

[28] F. Smith, Lifetime matrix in collision theory, Phys. Rev. **118**, 349 (1960).

[29] M. Davy, Z. Shi, J. Wang, X. Cheng, and A. Z. Genack, Transmission Eigenchannels and the Densities of States of Random Media, Phys. Rev. Lett. **114**, 033901 (2015).

[30] M. Davy, Z. Shi, J. Park, C. Tian, and A. Z. Genack, Universal structure of transmission eigenchannels inside opaque media, Nat. Commun. **6**, 6893 (2015).

[31] R. Pierrat, P. Ambichl, S. Gigan, A. Haber, R. Carminati, and S. Rotter, Invariance property of wave scattering through disordered media, Proc. Natl. Acad. Sci. USA **111**, 17765 (2014).

[32] R. Savo, R. Pierrat, U. Najar, C. Rémi, S. Rotter, and S. Gigan, Mean path length invariance in multiple light scattering, Science **358**, 765 (2017).

[33] S. Fan and J. Kahn, Principal modes in multimode waveguides, Opt. Lett. **30**, 135 (2005).

[34] M. B. Shemirani, W. Mao, R. A. Panicker, and J. M. Kahn, Principal modes in graded-index multimode fiber in presence of spatial- and polarization-mode coupling, J. Lightwave Technol. **27**, 1248 (2009).

[35] J. Carpenter, B. J. Eggleton, and J. Schröder, Comparison of principal modes and spatial eigenmodes in multimode optical fibre, Laser Photon. Rev. **11**, 1600259 (2017).

[36] See Supplemental Material at http://link.aps.org/supplemental/10.1103/PhysRevA.97.021801 for details on: (1) the experimental data treatment via Fourier filtering to stabilize the phase derivative of the scattering matrix; (2) the extraction of the q operator for non-quadratic or singular transmission matrices T; and (3) a strategy for demixing particlelike scattering states belonging to path bundles of the same or very similar lengths.

[37] J. Unterhinninghofen, U. Kuhl, J. Wiersig, H.-J. Stöckmann, and M. Hentschel, Measurement of the Goos-Hänchen shift in a microwave cavity, New J. Phys. **13**, 023013 (2011).

[38] S. Barkhofen, J. J. Metzger, R. Fleischmann, U. Kuhl, and H.-J. Stöckmann, Experimental Observation of a Fundamental Length Scale of Waves in Random Media, Phys. Rev. Lett. **111**, 183902 (2013).

[39] J. Salz, Digital transmission over cross-coupled linear channels, AT T Techn. J. **64**, 1147 (1985).

[40] H. Sampath, S. Talwar, J. Tellado, V. Erceg, and A. Paulraj, A fourth-generation MIMO-OFDM broadband wireless system: Design, performance, and field trial results, IEEE Commun. Magaz. **40**, 143 (2002).